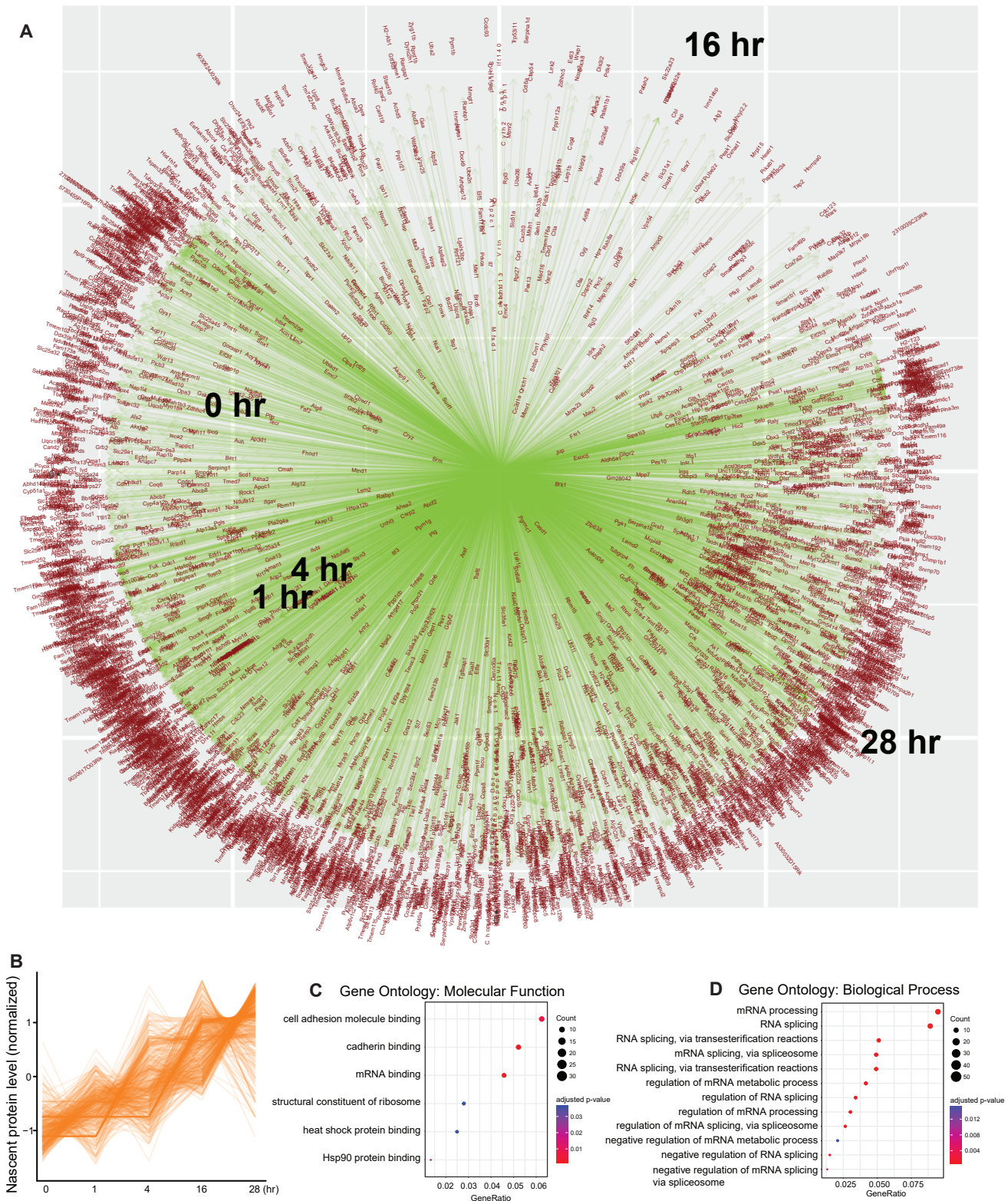


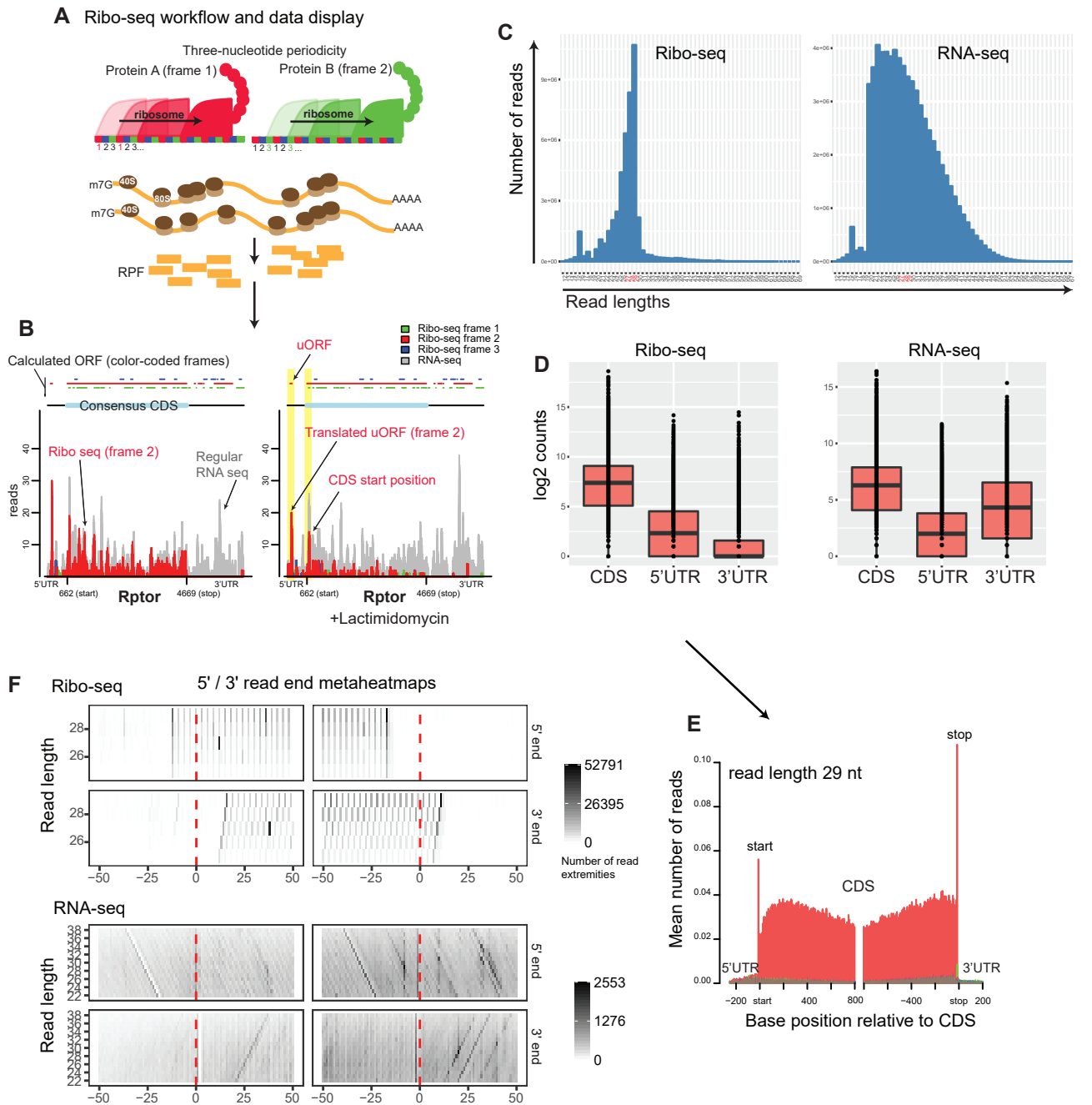
Supplemental Figure 1



Supplemental Figure 1.

(A) Magnified view of Main Figure 2B (unflatten). See also Supplemental Table 1. Protein symbols were converted to gene symbols for ease of comparison with subsequent ribo-seq data. (B) Cluster analysis was performed and nascent proteins that trended upward overtime are shown (each orange line indicates one protein; n=870 out of ~6,000 nascent proteins detected belong to this cluster). (C and D) Pathway enrichment analysis using Gene Ontology terms. The size of the dots reflects the number of proteins attributed to the Gene Ontology term, and the color of the dots denotes adjusted p-values.

Supplemental Figure 2

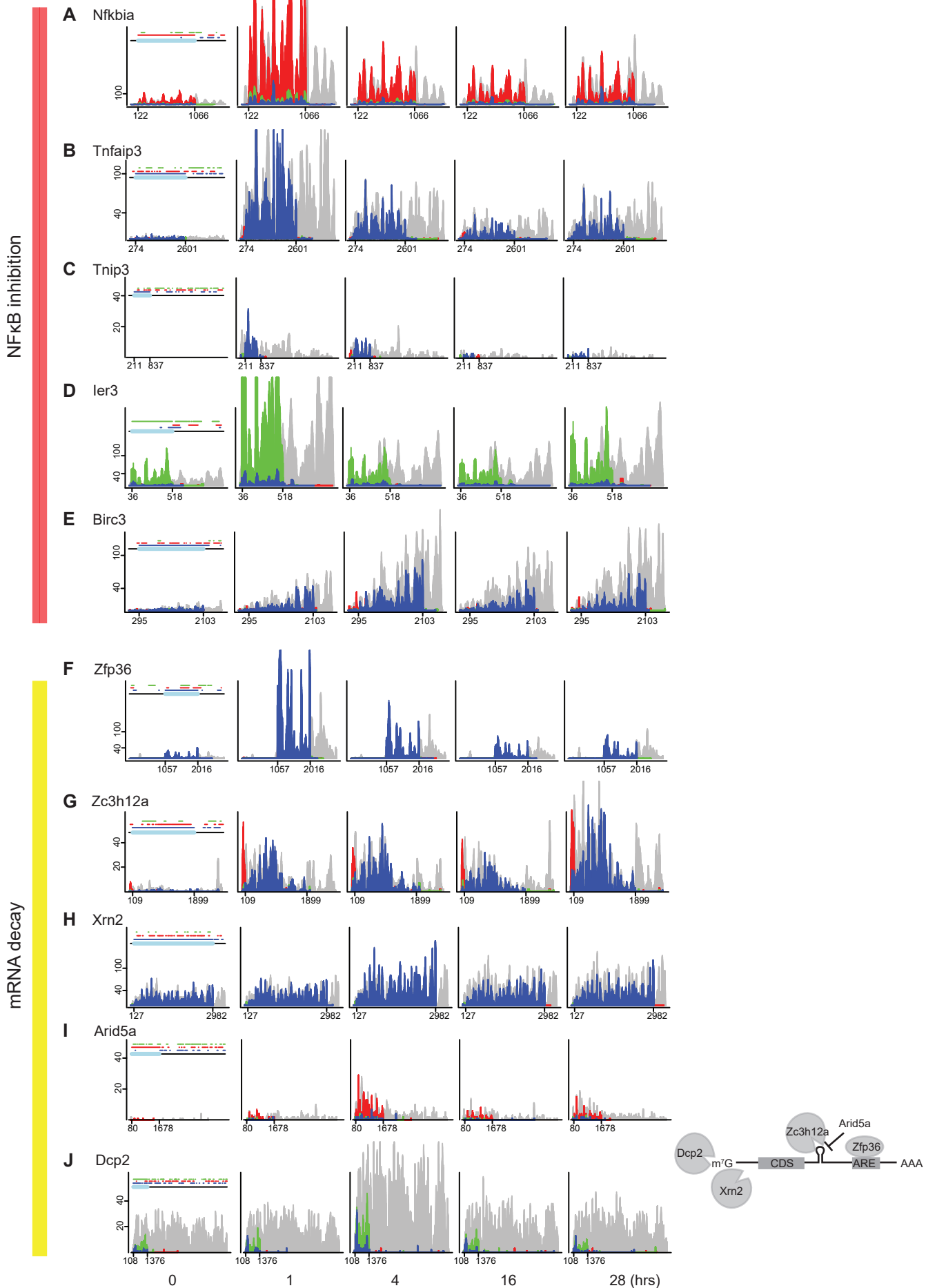


Supplemental Fig. 2.

(A and B) Ribo-seq schematic. Ribosome protected mRNA fragments (RPF; median 29 nucleotides) are isolated and sequenced. Ribosomes advance their position 3 nucleotides at a time. Thus a ribosome on a given mRNA remains in a specific frame (frame 1, 2, or 3) throughout its translation process. The precise periodic movement of ribosomes makes it possible to determine start and stop positions, frame and density (coverage). RNA-seq reads (gray) and ribo-seq reads (red, blue, green) were mapped to the GRCm38-mm10 mouse transcriptome. X-axis denotes mRNA positions. Y-axis denotes read coverage. Green, red, blue colors in the histogram correspond to ribosome frames 1, 2, and 3, respectively. On the top, calculated open reading frame positions (ORF; defined by ATG start codon, TAG/TAA/TGA stop codons) and their associated frame colors are shown (frames determined by modulo operation: RPF left end position % 3). Annotated consensus coding sequence (CCDS) is highlighted in light blue on the top and its start and stop positions are shown on the x-axis. Note that CCDS frame can be 1, 2, or 3, depending on the position of CCDS in that particular transcript. As an example, ribo-seq analysis of gene *Rptor* with and without lactimidomycin is shown in (B). Lactimidomycin halts the movement of ribosomes engaged at the initiation site (but not the elongating ribosomes), and therefore highlights the initiation position. As shown, CCDS from the GRCm38-mm10 mouse transcriptome is displayed in light blue on the top with positions 662 (start) and 4669 (stop) on the x-axis. Note that one of the calculated ORFs in frame 2 (red) matches up to this annotated region. Almost all ribosome reads mapped to this region are indeed in frame 2 (red), a reflection of high ribosome movement fidelity (triplet periodicity; ribosomes “jump” 3 nucleotides at once instead of plowing through one nucleotide at a time). Note also the presence of a translated upstream ORF in frame 2 (red) as indicated by: 1. the prominent signal that remains elevated after lactimidomycin treatment, and 2. the presence of the calculated ORF in frame 2 spanning the corresponding region. (C) Length distribution of mouse kidney RPFs (left). RPF distribution peaked at 29 nt as expected. RNA-seq reads (right) underwent additional fragmentation to provide similar fragment sizes to the RPF reads. (D) Boxplots of read coverage on the CDS, 5'UTR, and 3'UTR regions for the entire protein coding genes. Since ribosomes are released at the stop codon, 3'UTR coverage in ribo-seq is minimal. (E) Histogram of RPF positions relative to the coding sequences for the entire protein coding genes. Only the 29 nt RPFs are shown for clarity. In this view, the blue and green frames are masked under the red color frame. Note the peak signals at start and end positions. These peaks occur due to differential regulation of initiation, elongation and termination, i.e., differences in the rate of ribosomal movement along mRNA. (F) 5' and 3' read-end metaheatmaps of ribo-seq and RNA-seq (read end counts density), demonstrating a transcriptome-wide 3-nucleotide periodicity in ribo-seq but not in RNA-seq.

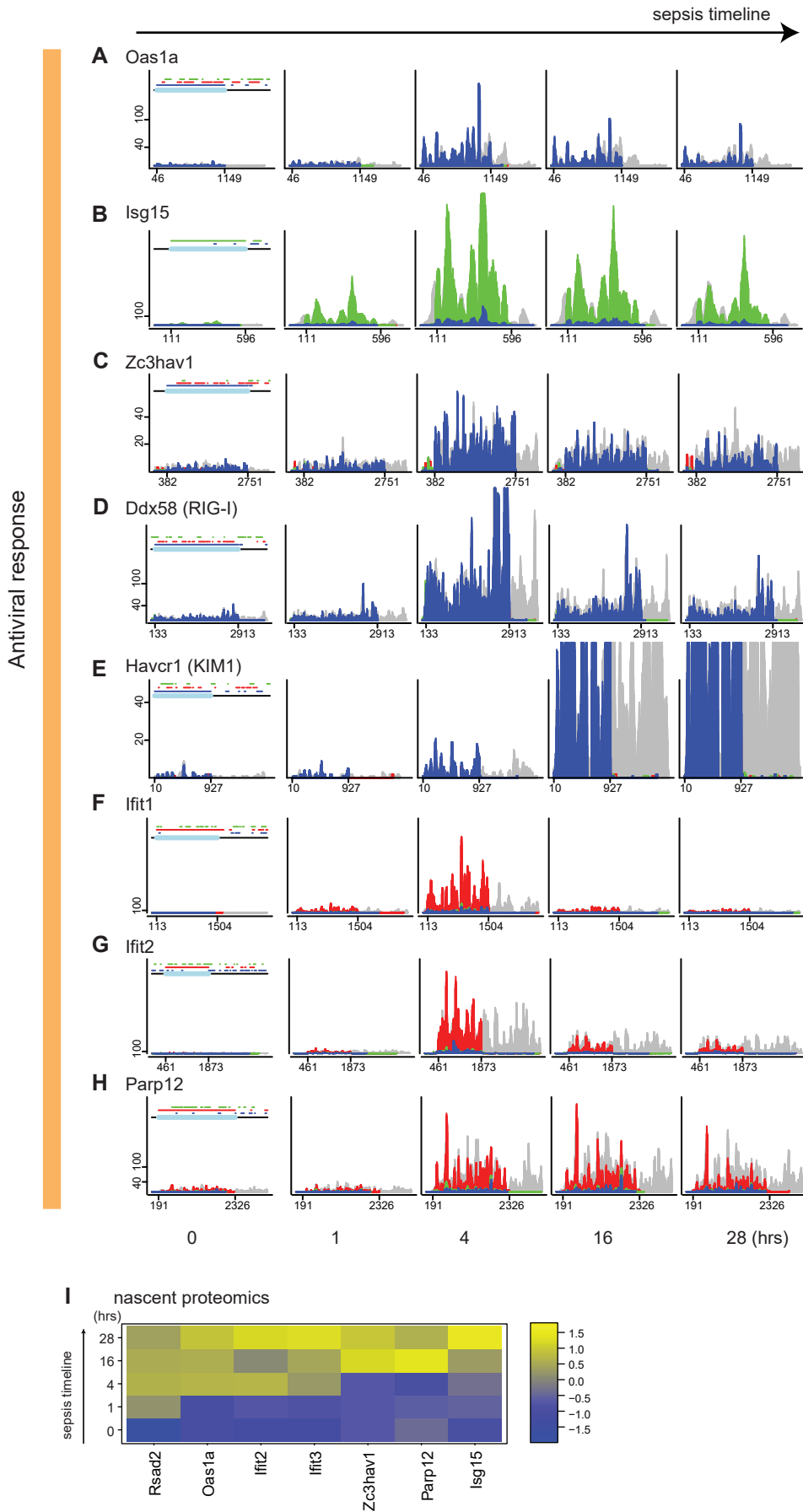
Supplemental Figure 3

Sepsis timeline →



Supplemental Fig. 3. a-j, Ribo-seq analysis of select genes involved in NFκB inhibition and mRNA decay machinery.

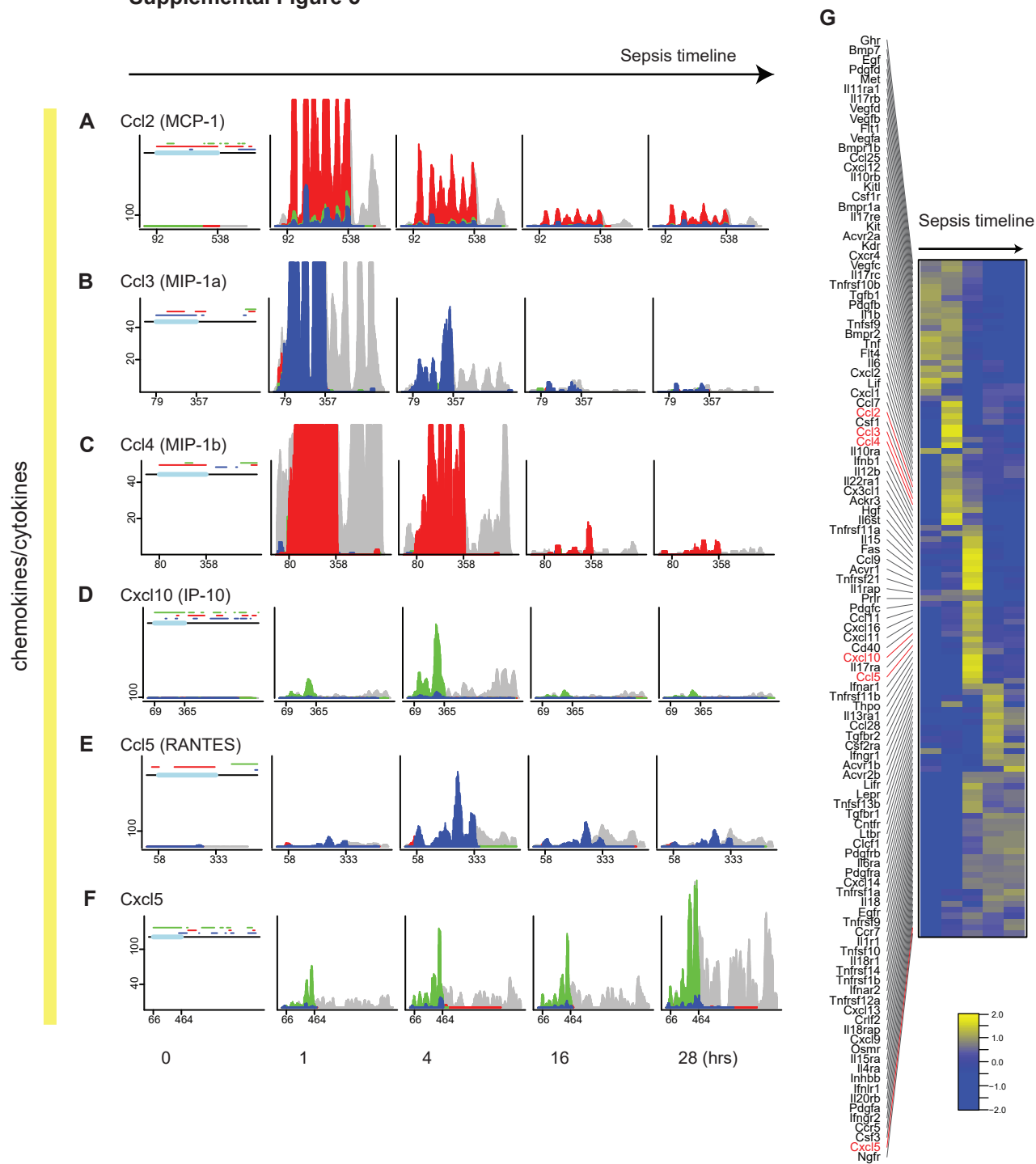
Supplemental Figure 4



Supplemental Fig. 4.

(A-H) Ribo-seq analysis of select genes involved in viral response pathways. (I) Pertinent nascent proteomics data are also shown.

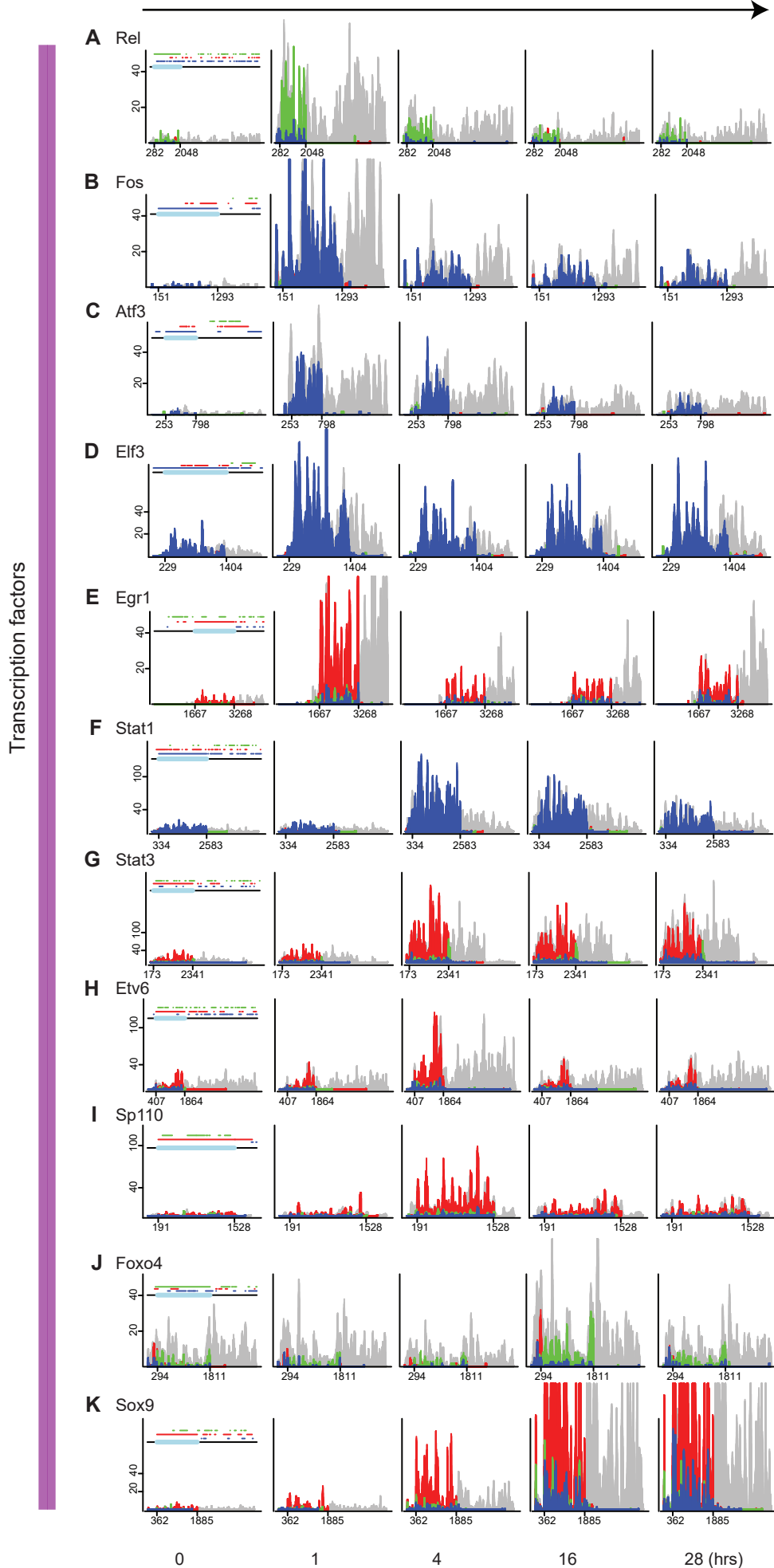
Supplemental Figure 5



Supplemental Fig. 5.

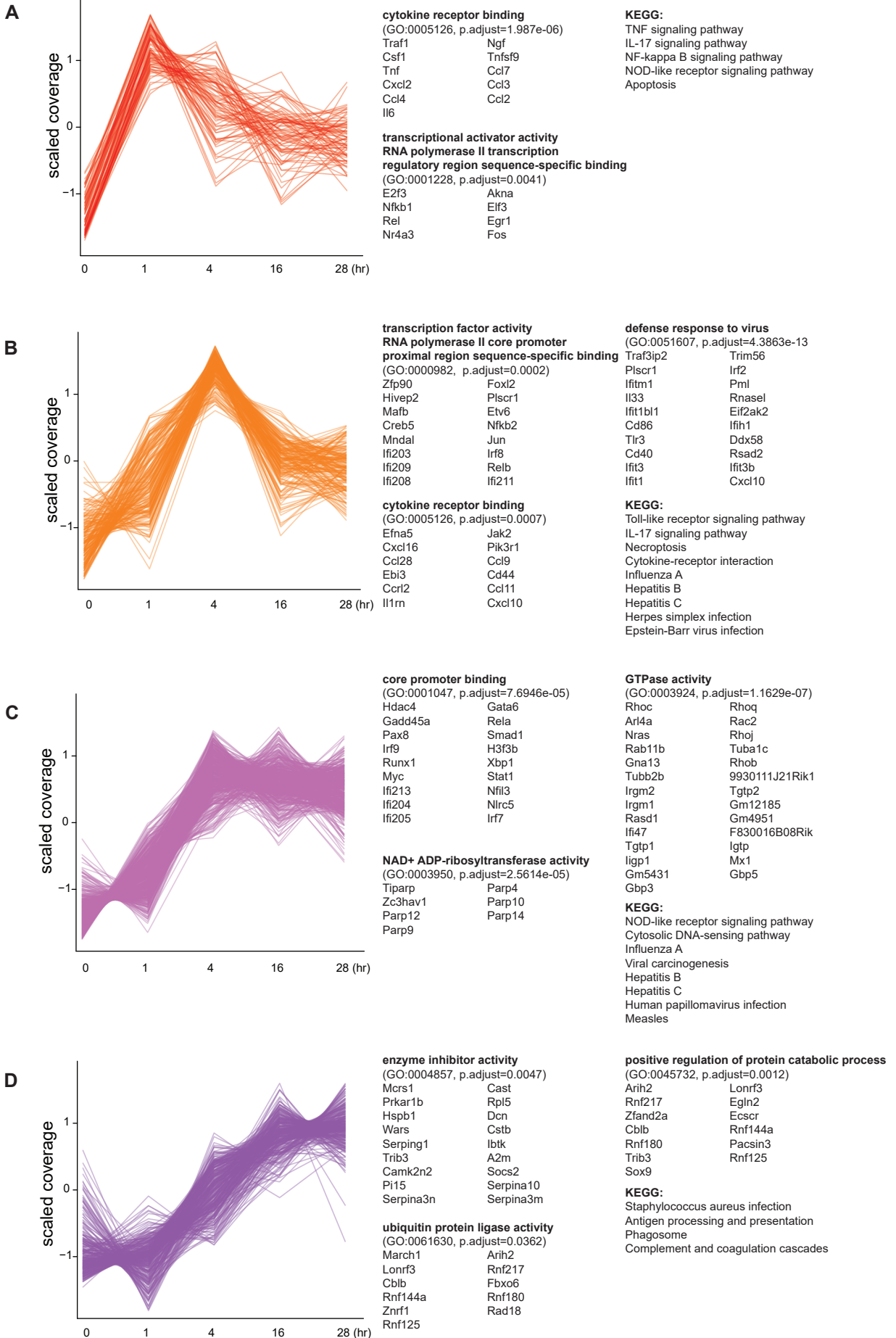
(A-F) Ribo-seq analysis of select genes involved in cytokine-cytokine receptor interaction.

(G) Summary of the cytokine-cytokine receptor interaction pathway (KEGG 04060) translato.



Supplemental Fig. 6. (A-K) Ribo-seq analysis of select transcription factors.

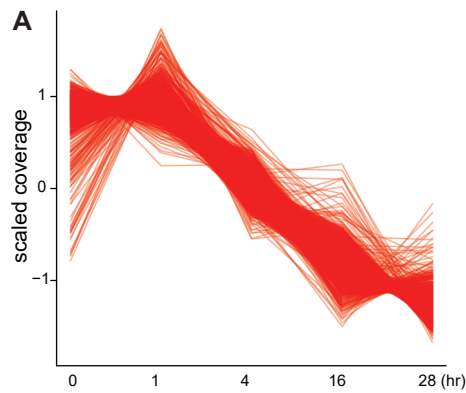
Supplemental Figure 7



Supplemental Fig. 7.

(A-D) Using translome counts data, unsupervised clustering analysis was performed. Four predominantly upswing clusters and corresponding pathway enrichment analysis are shown.

Supplemental Figure 8



cofactor binding
(GO:0048037, p.adjust=1.4471e-07)

Acbd5	Tkt
MaobDecr1	Dus2
Acat1	Fasn
Etfa	Htatip2
Shmt1	Sirt4
Ndufs7	Acad9
Acadm	Sdr39u1
Sirt5	Phykp1
Tyms	Mmachc
Agps	Ldh3a
Vkorc1	Gpd1
Ddo	Srd5a1
Pygm	

protein folding
(GO:0006457, p.adjust=1.8907e-05)

Tmx1	Pdia3
Tmx3	Prdx4
Fkbp9	Cdc37
Ero1lb	Erp44
Erp29	Fkbp3
Ppif	Hsp90ab1
Hspd1	Mkks
Hsph1	Fkbp4

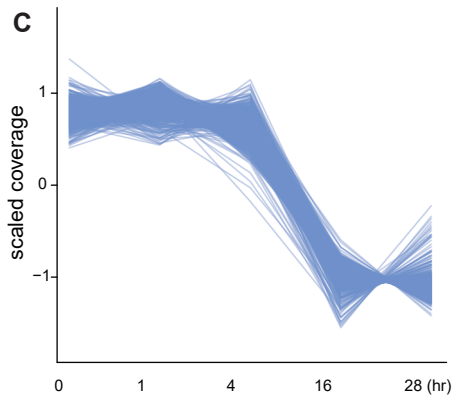
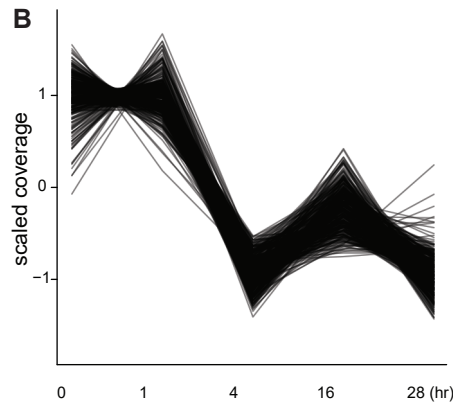
damaged DNA binding
(GO:0003684, p.adjust=0.036)

Nbn	Msh2
Xrcc1	Neil1
Polh	Poli
Msh3	

negative regulation of DNA metabolic process
(GO:0051053, p.adjust=0.0225)

Nbn	Nudt16l1
Pds5a	Ficn
Msh2	Xrcc1
Dffa	Papd5
Zfp830	Msh3
Tipin	

KEGG
AMPK signaling pathway
Hedgehog signaling pathway
cGMP-PKG signaling pathway



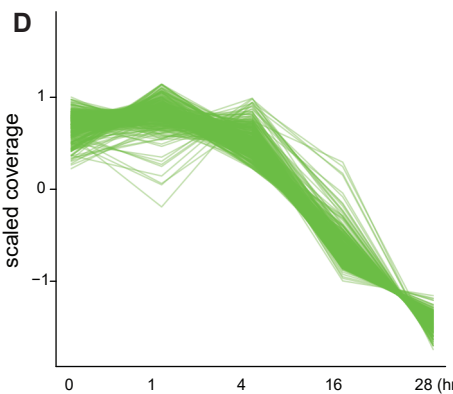
oxidoreductase activity
(GO:0016614, p.adjust=3.4366e-18)

Adhfe1	Mdh2
Adh5	Dhrs7b
Idh3b	Bdh1
Hsd17b10	Mdh1
Hadh	Me1
Akr1a1	Akr7a5
Grhpr	Bdh2
Nsdhl	Ptgr1
L2hgdh	Srd5a2
Dhdh	Idh1
Akr1e1	Akr1c21
Hao2	Hsd3b3

electron transfer activity
(GO:0009055, p.adjust=1.6263e-13)

Uqcrcq	Did
Sdha	Cox5a
Sdhc	Sdhb
Uqcfrs1	Cox7a2
Cyc1	Ndufa4
Ndufa12	Uqcqh
Ndufs1	Nqo2

KEGG
Oxidative phosphorylation
Citrate cycle (TCA cycle)



small molecule biosynthetic process
(GO:0044283, p.adjust=3.1607e-07)

Coq4	Gls
Coq3	Apoa4
Tecr	Oxsm
Pdk2	Pcbd2
C1qtnf12	Pdss2
Srr	Coq9
Mvk	Uros
Pecr	Kmo
Cyp51	Egf
Bhmt2	Acss2

fatty acid metabolic process
(GO:0006631, p.adjust=3.1888e-07)

Mapk14	Auh
Apoa4	Acad11
Tecr	Oxsm
Trnxb	Acss1
Pdk2	Echdc1
Acaa1b	Prkag3
Cyp2d12	Pecr
Acnat1	Cyp2d26
Acss2	

nuclear outer membrane-endoplasmic reticulum membrane network

(GO:0042175, p.adjust=2.9533e-06)

Tytw1	Tkt	Tmx1	Lmf2
Ndufs2	Dad1	Pdia3	March6
Acadsb	Dnajc3	Erlin2	Tmx3
Hmgcr	Piga	Rab14	Ptdss2
Creg1	Abcb9	Ddost	Pigu
Parp1	Slc9a6	Nomo1	Ddrgrk1
Fmo2	Aldh3a2	Sptssa	Pomt2
Fdxr	Ero1lb	Sdf2	Dolk
Kdm1b	Alg8	Erp44	Rab1b
Dhcr24	Tmem33	Hmgcr	Hsp90b1
Dhfr	Vapb	Pkd2	Canx
Hsd11b2	Pigb	Wis	Pigq
	Epm2a	Dhcr7	Tmem178
	Alg6	Itpr2	Reep6
	Ndrgr4	Pigf	Pyurf
	Hacd4	Cfr	

mitochondrial translation
(GO:0032543, p.adjust=4.7558e-06)

Chchd4	Mrps16	Mrps27	Mrlp58
P4hb	C1qbp	Mtg1	Coa3
Pdia4	Mrps11	Uqcq1	Gatb
Dnajb14	Mrps11	Mars2	Yars2
Hsp90b1	Canx	Mtg2	Ptcd3
Canx	Hspe1	Tsfn	
Hspe1	Rmnd1		
Chordc1			

KEGG
Pantothenate and CoA biosynthesis
Peroxisome
Protein processing in ER
GPI-anchor biosynthesis

smoothened signaling pathway
(GO:0007224, p.adjust=0.0112)

Ift88	Prkacb	Evc2
Cdon	Wdr19	2700049A03Rik
Gas1	Sufu	Wnt7b
1810043G02Rik	Cc2d2a	Sall3

ciliary part
(GO:0044441, p.adjust=0.0188)

Cep290	Ift88	Prkacb
Evc2	Bbs5	Wrap73
Wdr19	Nek4	2700049A03Rik
Cfap20	Cby1	Nphp1
1810043G02Rik	Sept4	Irs1
Cc2d2a	Prkar2b	Ak1
Crocc		

active transmembrane transporter activity
(GO:0022804, p.adjust=5.3511e-26)

Ldhd	Slc1a1	Atp6v1a
Rdh5	Abcb8	Clcn5
Akr1b10	Atp5d	Atp5g3
Rdh16	Atp6ap1	Tfrc
Dhrs4	Slc26a4	Slc25a3
Dhrs11	Atp5o	Atp2b4
Dcxr	Clcn3	Atp5f1
Cryl1	Atp5c1	Abcb7
Dhrs3	Atp6v0e2	Slc5a2
Miox	Slc16a2	Abcc4
Sord	Slc16a4	Slc22a18
	Slc22a2	Slco1a1
	Slc6a13	Slc22a30
	Slc5a9	Abcc6
	Slc33a1	Slc17a3
Cox8a	Abcc9	Slc7a13
Uqcrc10	Abcc2	Slc22a28
Cox7b	Slc5a11	Slc7a7
Cox6c	Slc22a22	Slc7a12
Fdx1	Slc47a1	Slc26a1
Uqcrcb	Slc16a7	Slc13a3
Cox7a1	Slc16a9	Slc8a1
		Atp5a1
		Abcb8
		Atp5d
		Atp6ap1
		Slc26a4
		Atp5o
		Atp5f1
		Abcb7
		Slc5a2
		Abcc4
		Slc22a18
		Slco1a1
		Slc22a30
		Abcc6
		Slc17a3
		Slc7a13
		Slc22a28
		Slc7a7
		Slc7a12
		Slc26a1
		Slc13a3
		Slc8a1
		Clcn5
		Atp5g3
		Tfrc
		Slc25a3
		Atp2b4
		Atp5e
		Tmco3
		Slc22a8
		Slc22a1
		Abcg2
		Slc44a
		Slc36a1
		Abca13
		Slc34a1
		Slc7a8
		Slc22a6
		Slc6a20b
		Slc6a4
		Slc16a12
		Slc10a2
		Slc26a7

cellular amino acid metabolic process
(GO:0006520, p.adjust=0.0002)

Acad8	Auh
Vars2	Gls
Uroc1	Aars2
Cars2	Tars2
Mpst	Scly
Nars2	Hibch
Acy1	Srr
Kmo	Mthfd1
Bhmt2	

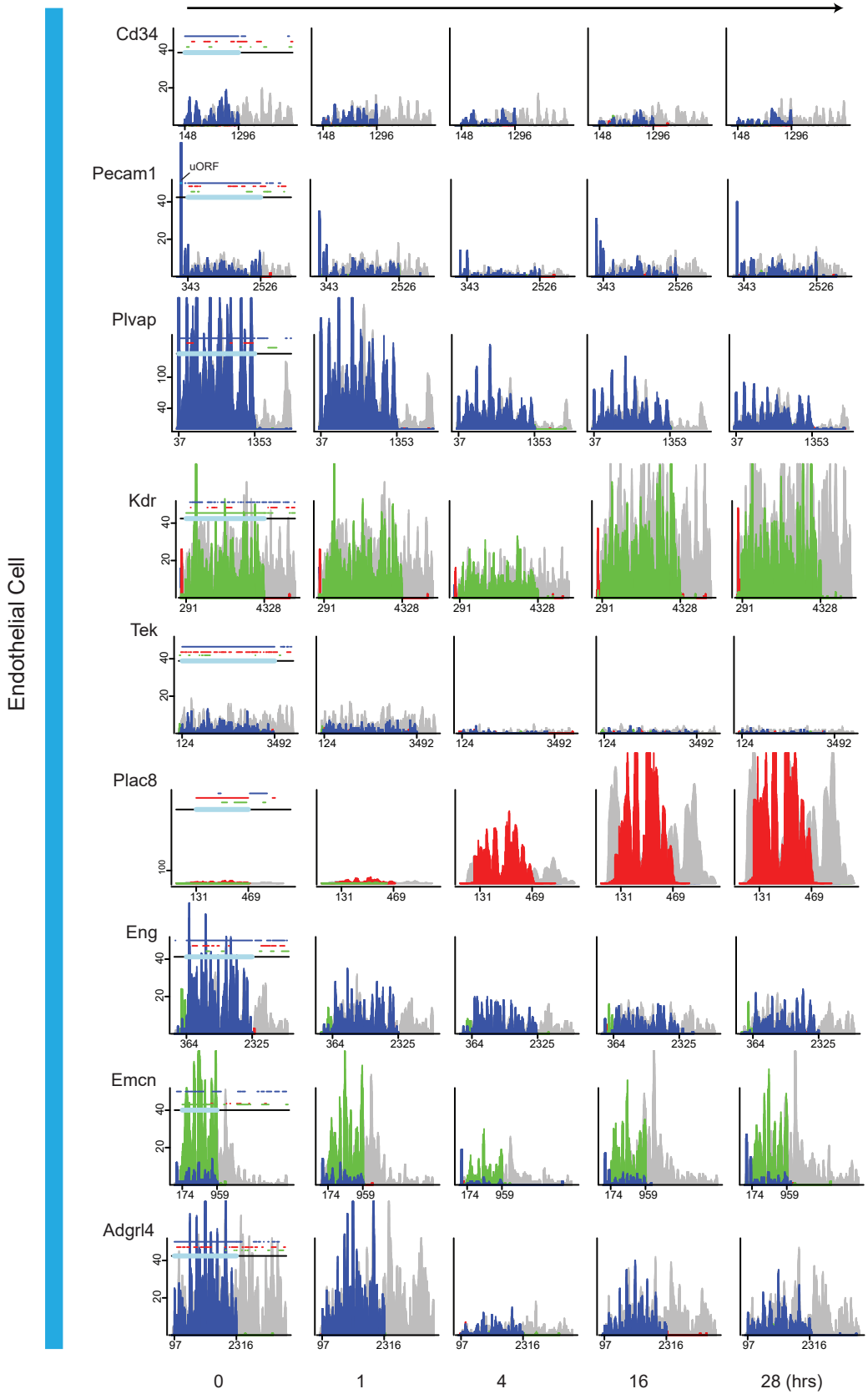
KEGG
Carbon metabolism
Sulfur metabolism
Folate biosynthesis
ECM-receptor interaction
Fatty acid metabolism
Proximal tubule bicarbonate reclamation
Valine, leucine and isoleucine degradation

Supplemental Fig. 8.

(A-D) Four predominantly down trending clusters and corresponding pathway enrichment analysis are shown.

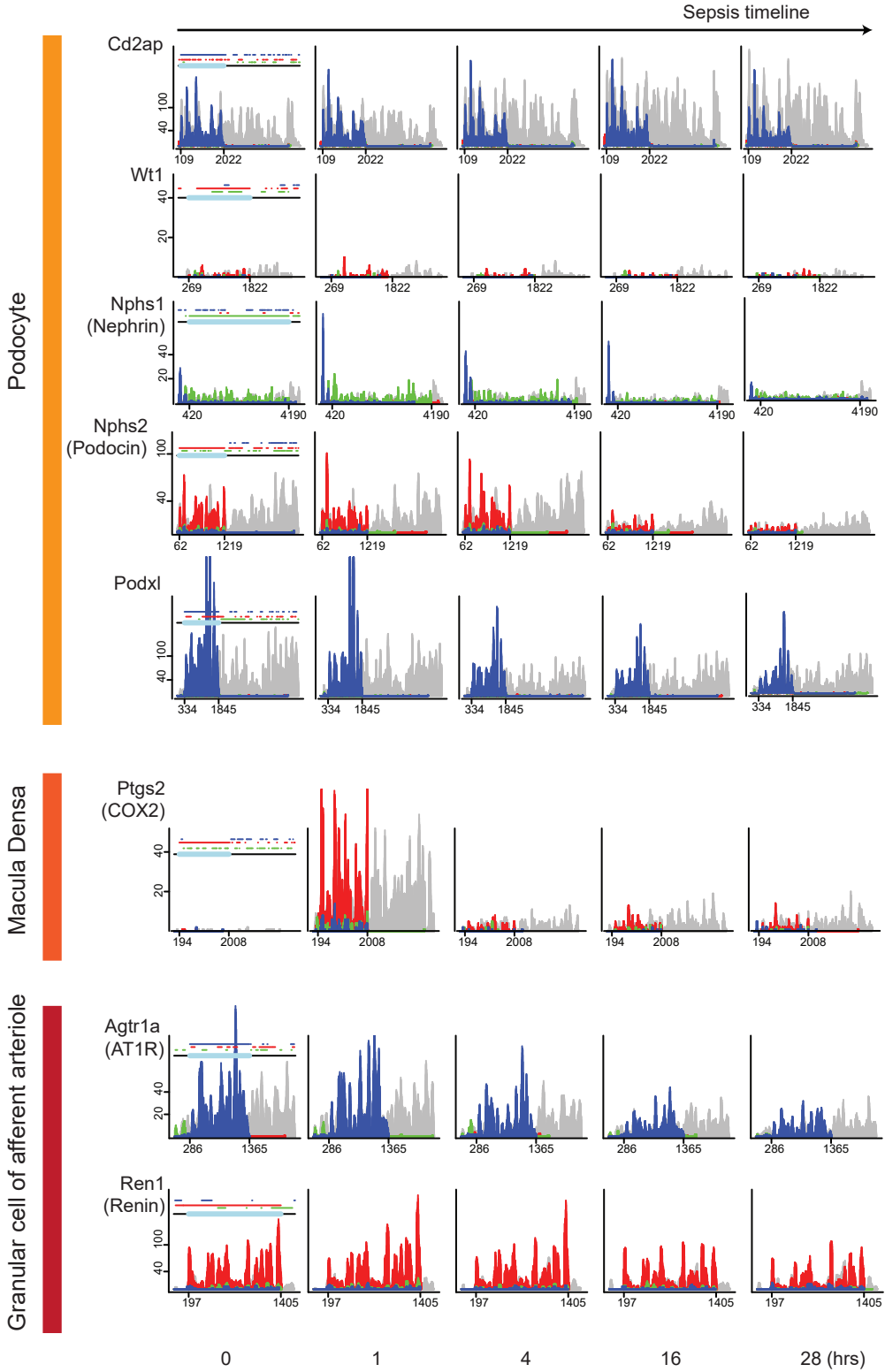
Supplemental Figure 9

Sepsis timeline



Supplemental Fig. 9. Ribo-seq analysis of select endothelial cell genes (38).

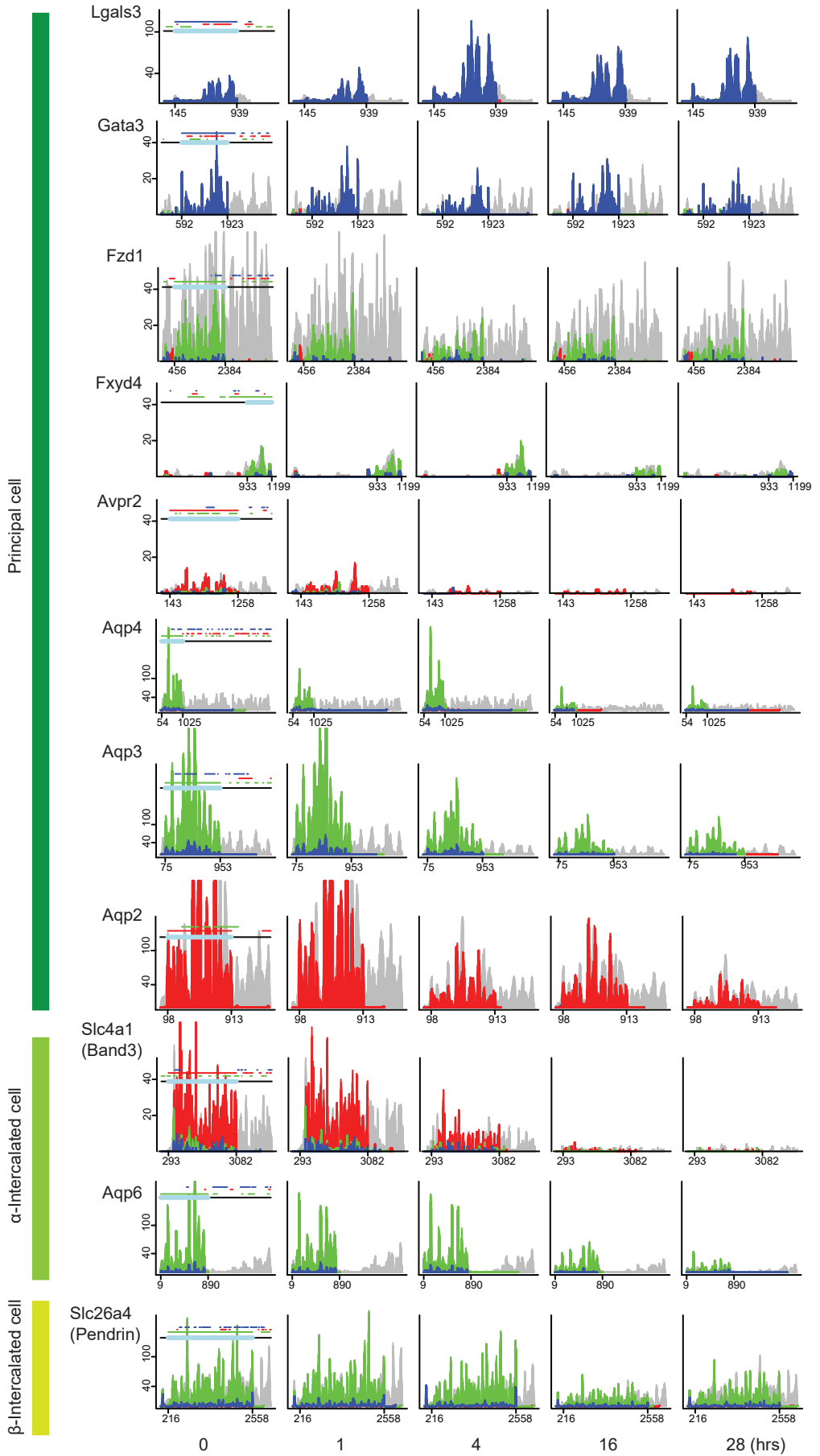
Supplemental Figure 10



Supplemental Fig. 10. Ribo-seq analysis of select genes (podocyte, macula densa, granular cell of afferent arteriole).

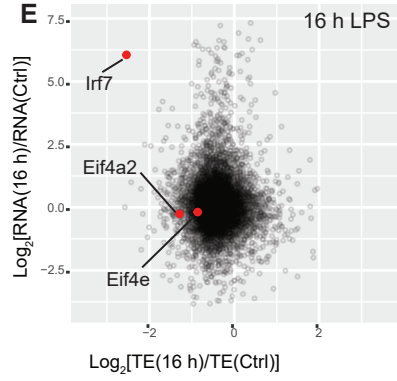
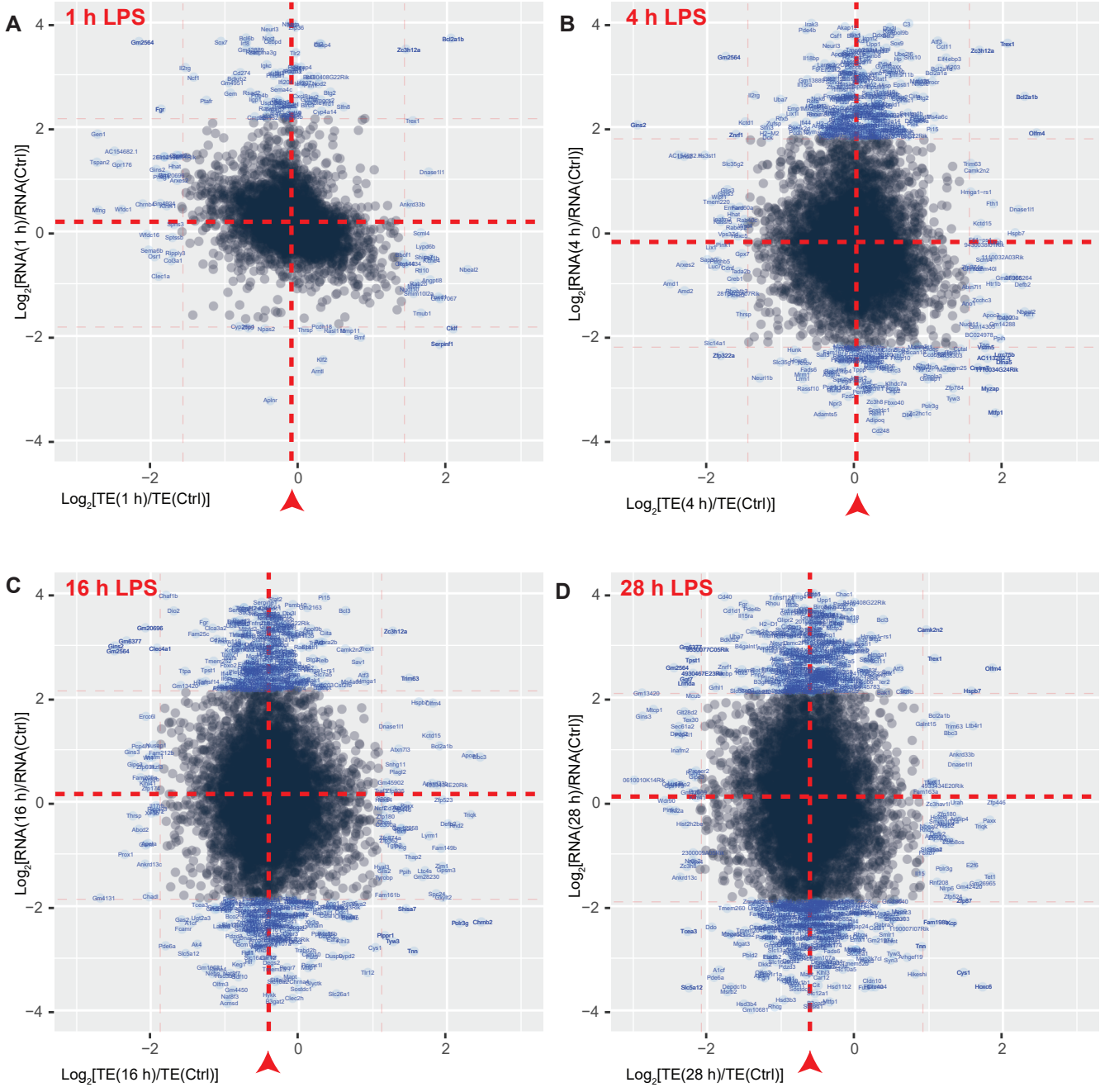
Supplemental Figure 11

Collecting Duct



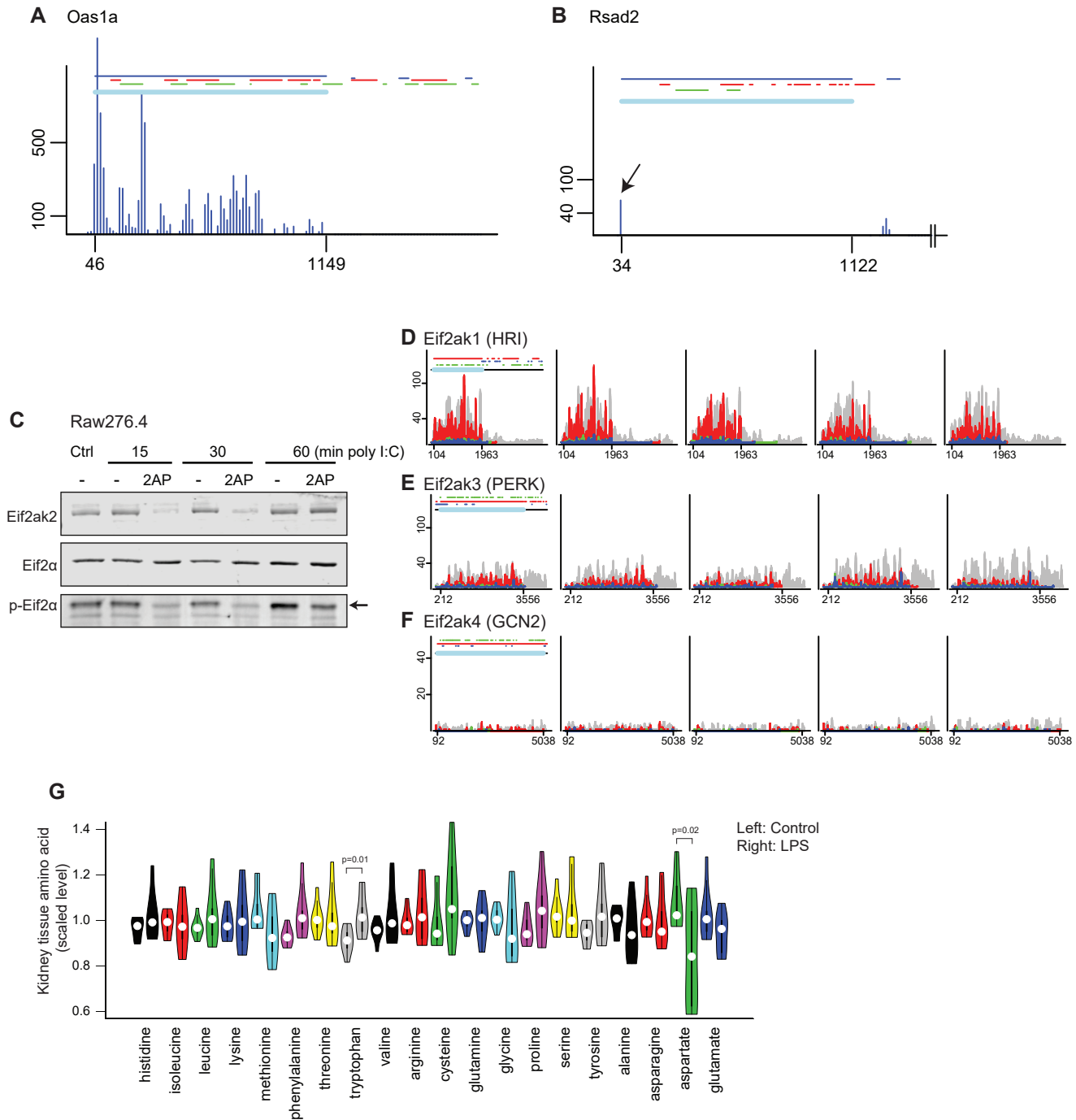
Supplemental Fig. 11. Ribo-seq analysis of select genes (collecting duct) (38).

Supplemental Figure 12



Supplemental Figure 12.
(A – D) Scatter plots of translation efficiency changes (TE, ribo-seq/RNA-seq; x-axis) and mRNA abundance changes (y-axis) under indicated time points. The dotted red lines depict overall translation efficiency and mRNA abundance changes (mean). Overall translation efficiency was decreased with LPS treatment (16 and 28 hrs, arrow heads) while overall mRNA abundance remained unchanged. Genes are annotated in blue when their fold change in translation efficiency is $> \pm 1.5$ and/or mRNA abundance fold change $> \pm 2$ as compared to the overall mean values. Note, some genes are located at extreme positions, mostly due to very low expression levels in control, and these genes are outside of the display ranges. One such example, Irf7, is shown in (E). Specific positions for Eif4e and Eif4a2 are also highlighted in red.

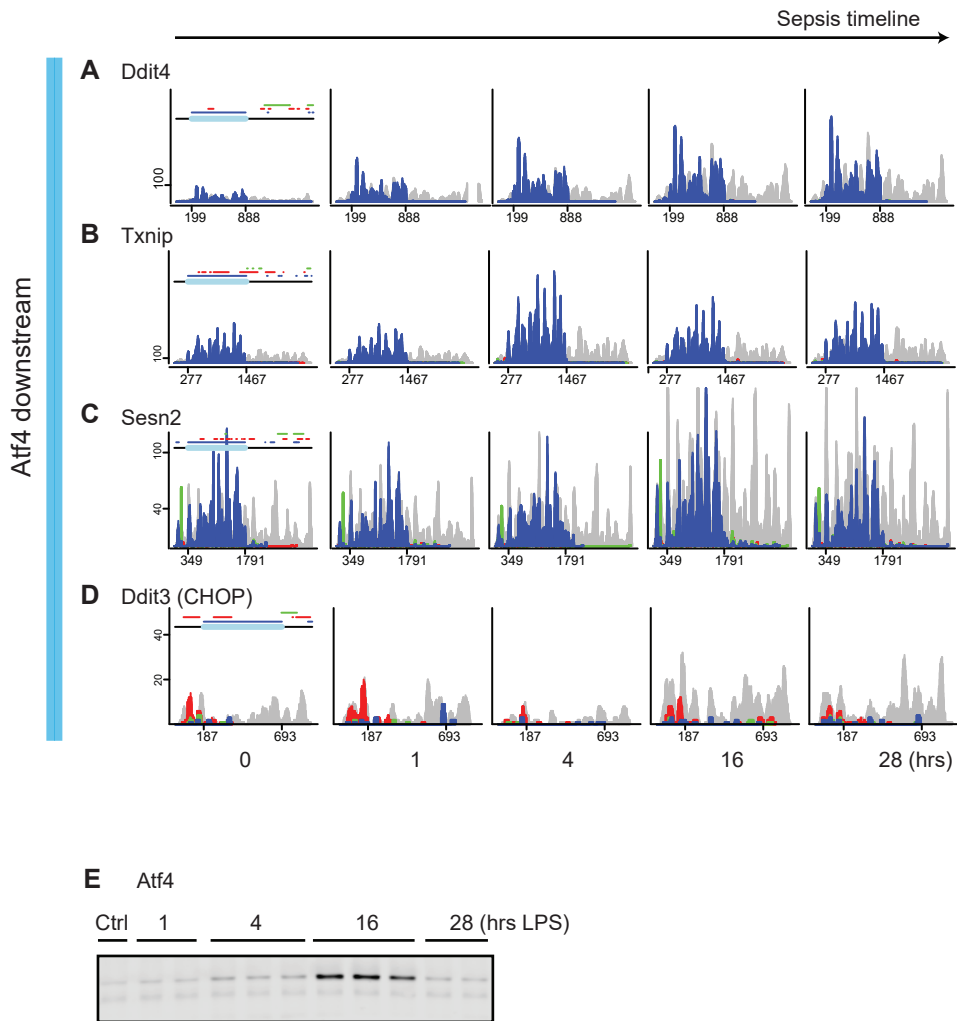
Supplemental Figure 13



Supplemental Fig. 13.

(A and B) Differential effect of lactimidomycin/puromycin is shown for Oas1a and Rsad2. Kidneys from control mice and mice treated with lactimidomycin/puromycin *in vivo* were harvested for ribo-seq. Arrow points to the Rsad2 initiation site where initiating ribosomes fixed by lactimidomycin withstood the effect of puromycin as expected. The rest of ribosomes on CDS fell off due to puromycin. In contrast, Oas1a ribosomes were largely unaffected by the lactimidomycin/puromycin treatment, indicating different kinetics. For clarity, only the blue frame signal is shown for both genes. RPF read coverages were binned every 15 nucleotides, thus the height of each histogram bar represents a sum of 15 nucleotide RPF coverage. Also note that short-term *in vivo* lactimidomycin/puromycin use was associated with incomplete isolation of initiation sites. Thus subtraction of lactimidomycin/puromycin treated reads from untreated reads was done to clearly illustrate their effect. (C) Western blot analysis of Raw 276.4 cells treated with 50 μ g/ml poly (I:C), a dsRNA analog and activator of TLR3 and PKR (Eif2ak2), with or without 1 mM 2-aminopurine (2-AP), a PKR inhibitor, for indicated durations. Arrow points to Ser51 phospho-Eif2 α . (D-F) Ribo-seq analysis of Eif2ak1, Eif2ak3, and Eif2ak4 revealed no significant changes in the translation of these kinases. (G) Violin plots of kidney tissue amino acid levels determined by metabolomics (left, control; right, LPS 5 mg/kg 24h for each amino acid). There was no systematic amino acid depletion, consistent with the lack of Eif2ak4 activation (n=8 for each condition).

Supplemental Figure 14

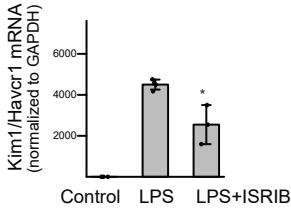


Supplemental Fig. 14.

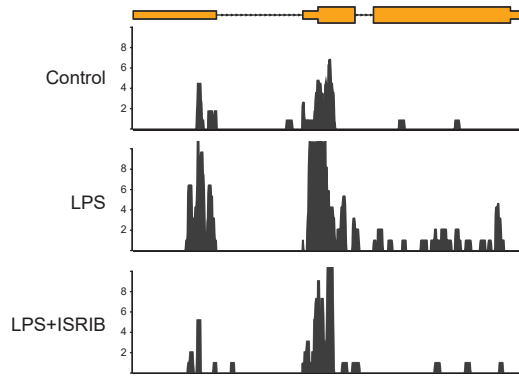
(A-D) Ribo-seq analysis of select genes downstream of Atf4. Note the discrepancy between Ddit3 mRNA (RNA-seq) and ribosome coverage signals (ribo-seq). (E) Western blot analysis of kidney tissue lysates for Atf4 under indicated conditions.

Supplemental Figure 15

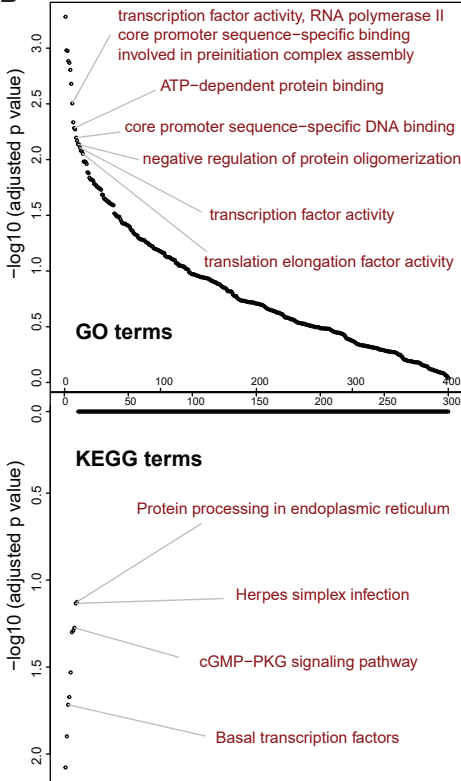
A



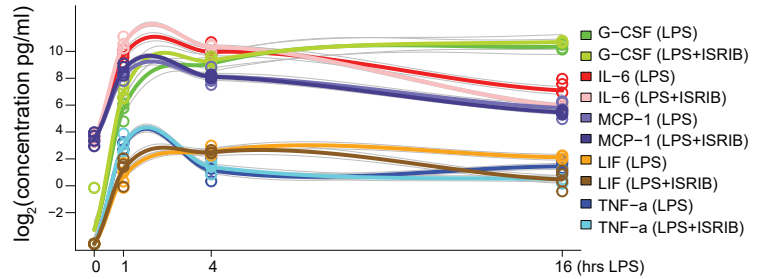
C Atf4 (chr15:80255184-80257545)



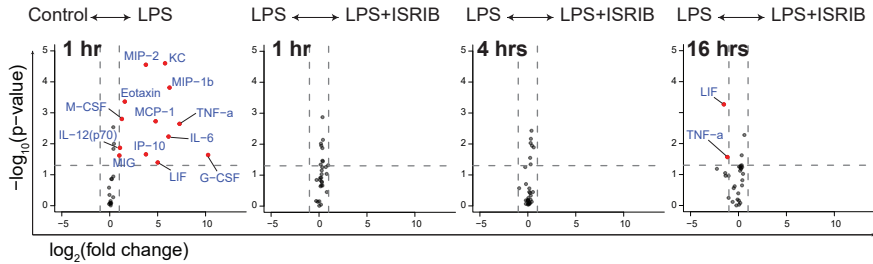
B LPS+ISIRB vs LPS



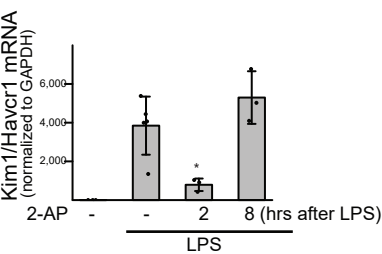
D



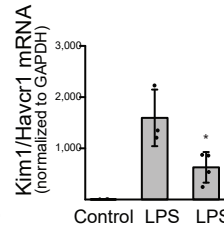
E



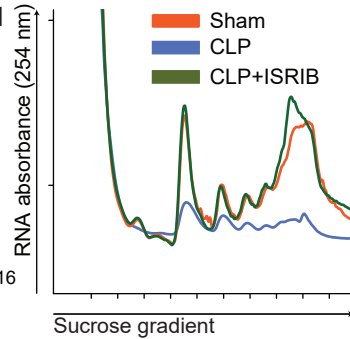
F



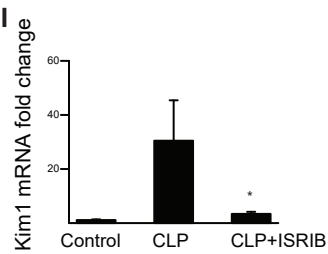
G



H



I

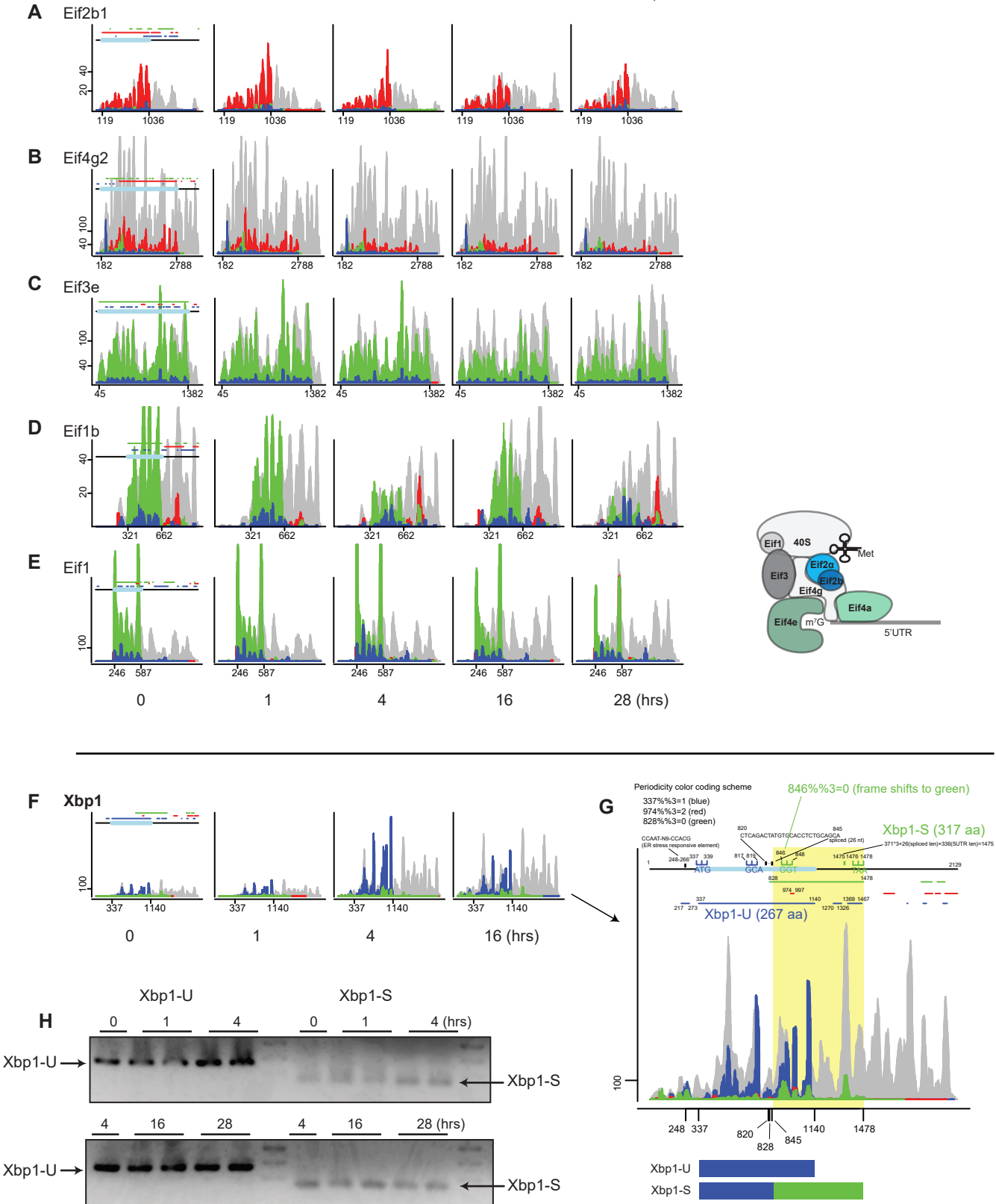


Supplemental Fig. 15.

(A) ISIRB or its vehicle were administered i.p. 1 hr after LPS and tissue Kim1/Havcr1 levels determined using quantitative PCR. (B) Pathway enrichment analysis comparing LPS+ISIRB and LPS+vehicle treatments (ribo-seq, n=3 per condition). Gene Ontology terms (GO) and Kyoto Encyclopedia of Genes and Genomics (KEGG) metabolic pathways are aligned in the order of statistical significance. (C) Representative Atf4 ribo-seq data under indicated conditions. Ribosome protected fragments (black) mapped to the Atf4 genome region are shown (exons in orange). (D-E) Tissue chemokine/cytokine levels determined by 32 multiplex assay (Milliplex). (D) Select cytokine/chemokine levels are shown to illustrate the similarities between LPS alone and LPS+ISIRB treated groups. ISIRB was administered 15 min after LPS. Locally weighted regression curve fitting was applied for generating the trajectories and error lines (gray). n=4 for each time point per group. (E) Volcano plots under indicated conditions. The vertical dotted lines demarcate ± 2 fold changes ($\log_2(2)$) and horizontal lines demarcate p value < 0.05 ($-\log_{10}(0.05)$). Genes above these thresholds are shown in red and annotated. (F) In vivo effect of 2-AP treatment (10 mg/kg ip) on sepsis-induced acute kidney injury as determined by tissue Kim1/Havcr1 mRNA levels. Mice were treated with LPS for 16 hrs with or without 2-AP administered at indicated time points. (G) Tissue Kim1/Havcr1 mRNA levels. Mice were injected with LPS followed 1 hr later by C16 (0.16 mg/kg ip) or its vehicle (DMSO). Kidneys were harvested 16 hrs after LPS. (H) Representative polysomal profiling of kidney extracts from mice under indicated conditions. Polysome-to-monosome ratios are 3.5, 2.7 and 3.7 for sham, CLP, and CLP+ISIRB, respectively. CLP for 16 hrs. ISIRB given at the time of abdominal closure. CLP, cecal ligation and puncture. (I) Tissue Kim1 mRNA levels under indicated conditions. *p<0.05 vs. LPS without ISIRB, 2-AP or C16 treatment.

Supplemental Figure 16

Sepsis timeline →

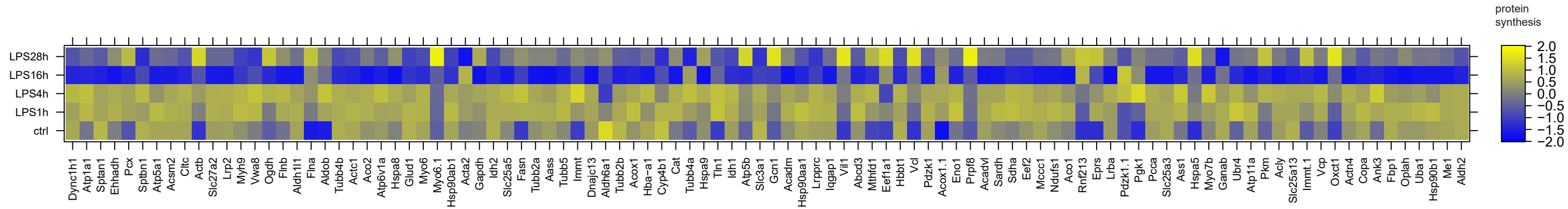


Supplemental Fig. 16.

(A-E) Ribo-seq analysis of select genes involved in cap-dependent translation initiation.

(F-G) Xbp1 undergoes unconventional splicing upon ER stress, which gives rise to the formation of Xbp1-S isoform (instead of unspliced Xbp1-U isoform). As illustrated in (G), the splicing causes a frameshift (-26 nt) such that the codon-periodicity frame changes from blue to green at position 846, thereby bypassing the Xbp1-U stop codon at 1140. In contrast, RPFs derived from unspliced Xbp1-U have blue frame periodicity throughout and stops at 1140. Xbp1-S level (as well as Xbp-U) increased with LPS challenge. (H) RT-PCR analysis of Xbp1 splicing, confirming the increase of Xbp-S at 4 and 16 hrs.

Supplemental Table 1



Nascent proteins are sorted by peptide-spectrum matches (PSMs) in decreasing order and 100 proteins are displayed on each page. Page 1 (this page) shows top 100 abundant nascent proteins by PSMs. Abundance values are log2 transformed and scaled for a set of proteins in each page. Protein names are converted to gene symbols for ease of comparison with ribo-seq data.

